Optimal Sizing on a Mission Profile of Isolated NPC DC-DC Converters using 3.3 kV SiC MOSFETs for Power Electronic Traction Transformers

Caroline Stackler, Florent Morel, Philippe Ladoux, Alexis Fouineau, François Wallart, Piotr Dworakowski

Optimal Sizing on a Mission Profile of Isolated NPC DC-DC Converters using 3.3 kV SiC MOSFETs for Power Electronic Traction Transformers

Caroline Stackler[1], Florent Morel[1], Philippe Ladoux[2], Alexis Fouineau[1], François Wallart[1], Piotr Dworakowski[1]

[1] ITE Supergrid Institute SAS, France
[2] Université de Toulouse, Laplace, France

Corresponding author: Piotr DWORAKOWSKI, piotr.dworakowski@supergrid-institute.com

Abstract

Multilevel converters, known as power electronic traction converters (PETT), are foreseen to replace bulky traditional on-board low frequency transformers (LFT) and two-level rectifiers in railway rolling stock. In addition to volume and weight reduction, a gain in the efficiency can be expected. This paper focuses on the isolated DC/DC conversion stage within the PETT, realised by a resonant converter, with 3-level NPC half-bridge primary and 2-level full-bridge secondary. Design is optimised both at nominal power and on a typical mission profile for a regional application. The comparison is carried out for 15 kV/16.7 Hz infrastructure and 2 MW PETTs using 3.3 kV SiC MOSFETs and nanocrystalline core transformers. The best MFT designs are achieved at 4 kHz when optimised on a mission profile and at 6 kHz when sized at rated power. A reduction of 13 % of the total energy loss on a typical journey can be obtained by optimising the design of the DC/DC converter on a mission profile rather than at nominal power.

1 Introduction

These past decades, a lot of works have been carried out on power electronic traction transformers (PETT) to replace bulky low frequency transformers (LFT) and two-level rectifiers in AC railway traction drives [1]–[6]. To reduce size and weight, these multilevel topologies include medium frequency transformers (MFT), operating typically at a few kilohertz.

A methodology has been previously developed to optimise the design of indirect modular topologies of PETTs (Fig. 1), and especially the design of the isolated DC/DC converter, at nominal power [7]–[9]. However, the traction drive load varies during a journey. For example, a typical mission profile can be divided in five phases [10]:

- an *acceleration phase*, used to reach the cruising speed of the train,
- a *cruising phase*, where the speed of the train is hold,
- a *coasting phase*, where the traction drive power is considered equal to the power of the auxiliaries, including the heating system and air conditioning,
- a *braking phase*, where power is transferred from the train to the catenary,
- a *stop phase*, during which the traction drive power corresponds to the power of the auxiliaries.

A typical 1 h journey mission profile for a regional application, based on *Regional 160* from [10] is considered here. In [9], a PETT is optimised at nominal power. The selected topology is referred to as HB/FB PETT, since its isolated DC/DC converter is composed of primary half bridge and secondary full bridge. The percentages of time of each phase and the repartition of the dissipated energy on the mission profile for this PETT topology are listed in Table 1.

Tab. 1: The 1h journey mission profile based on *Regional 160* from [10] and energy loss in the HB/FB PETT topology optimised at nominal power presented in [9]

Phases	% of time	Energy loss
Acceleration	8.2 %	192 kWh
Cruising	23.6 %	140 kWh
Coasting	48.0 %	168 kWh
Braking	4.6 %	76 kWh
Stop	15.6 %	54 kWh
Total	100.0 %	630 kWh

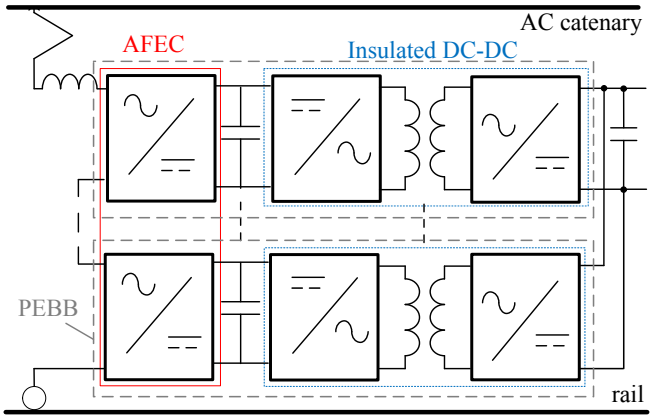

Fig. 1: Diagram of an indirect PETT topology

According to Table 1, one can notice that the energy loss during cruising, coasting and stop is non negligible on a typical journey. According to [9], the DC/DC converter power loss at low power is quite high. Lower losses can thus be expected for the design optimised on the mission profile. In this paper, optimisations of isolated DC/DC converters in a PETT, realised at nominal power and on the mission profile, are compared.

The PETT topology considered in this study is presented in section 2. Section 3 is dedicated to the methodology used to optimise the design of the isolated DC/DC converter either at nominal power, or on a mission profile. In section 4, some results, obtained for the regional application mentioned above, are presented. Some conclusions and perspectives close the paper.

2 PETT topology

A typical diagram of indirect modular PETT topologies with intermediate DC buses is depicted in Fig. 1. It is composed of an active front end converter (AFEC) connected to the overhead line through an input filter (either an inductor or a LCL filter [6], [11], [12]). To withstand the supply voltage, the AFEC is constituted of cascaded converters. The AFEC DC side supplies intermediate buses, on which are connected isolated DC/DC converters, including a medium frequency transformer. The output sides of the isolated DC/DC converters are in parallel on a traction bus. Afterwards, a power electronic building block (PEBB) is defined as an elementary isolated AC/DC converter between the input filter and the traction DC bus. A minimum number of PEBBs, fixed by the intermediate voltages, and so by the breakdown voltage of power semiconductor devices, is required to withstand the infrastructure voltage.

The considered DC/DC converter topology results from previous studies [8], [9]. A resonant single active bridge (R-SAB) (see Fig. 2 and Fig. 3), also known as series resonant converter (SRC) or resonant LLC converter, is investigated. It operates in discontinuous conduction mode (DCM), i.e. with a switching frequency lower than the resonant frequency, to maximise the efficiency. Three level NPC bridges have been considered in the input multilevel AC/DC converter and in the DC/DC primary. For a given semiconductor breakdown voltage, a higher intermediate bus voltage can thus be set compared to two level bridges, and the numbers of PEBBs and MFTs can be reduced. To minimise the number of semiconductors, without overly lowering the efficiency, half bridges are considered in the primary of the DC/DC converter and two level full bridges in the secondary [9]. To simplify the control, the 3-level NPC structure is used only to increase the intermediate voltage: both primary and secondary bridges are controlled in square wave modulation (i.e. both high-side switches receive the same control order; similarly, low-side switches are controlled synchronously). Nanocrystalline C-core transformers are considered as they lead to lower losses in the isolated DC/DC converter compared to ferrite MFTs for given weight and volume constraints [8].

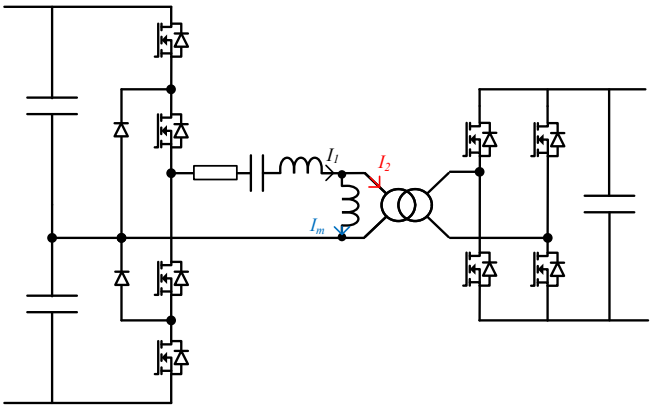

Fig. 2: Diagram of the R-SAB considered in the study. The secondary bridge operates as a diode bridge in traction. The primary bridge operates as a diode bridge in braking.

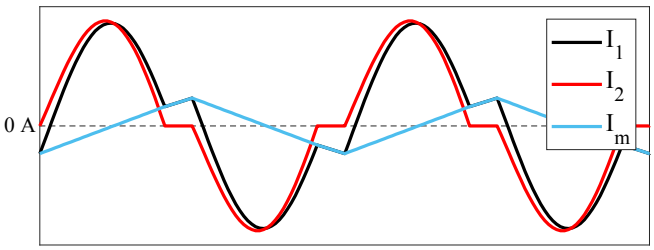

Fig. 3: Current waveforms in a R-SAB in DCM (low magnetising inductance to highlight the impact of the magnetising current) in a R-SAB in DCM

3 Sizing methodology

The sizing methodology, developed to maximise the efficiency of the DC/DC converter at rated power, under mass and dimension constraints, has been previously presented in [7]–[9]. The generalised flowchart, adapted for an optimisation on a mission profile, is shown Fig. 4.

To limit the switching losses, the MOSFETs are turned-on at zero voltage (ZVS). To do so, the C_{ds} capacitances of the MOSFETs have to be charged and discharged during the dead time. The current in the MOSFET during the switching, corresponding to the magnetising current in discontinuous conduction mode, has thus to be high enough. A maximum value of the magnetising inductance of the MFT is then required to ensure ZVS operation and to limit the switching losses [13].

In single active bridge mode, only one of the DC voltages, either the intermediate bus voltage or the traction bus voltage, can be controlled thanks to the input AC/DC stage (AFEC). The uncontrolled DC

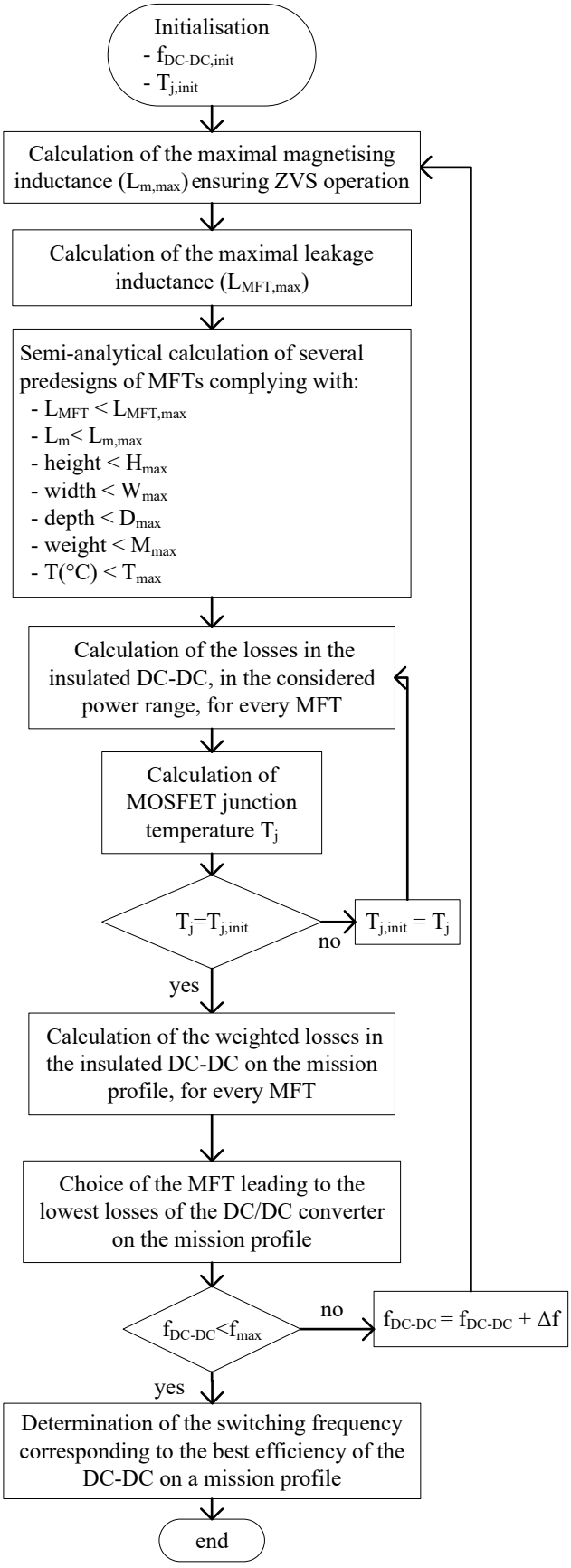

Fig. 4: Flowchart of the sizing methodology of an isolated DC/DC converter on a mission profile

voltage varies in function of the power absorbed on the traction bus and of the impedance of the AC link. To limit the voltage drop, the leakage inductance of the MFT is thus restricted.

The constraints on the MFT, i.e. the maximum leakage and magnetising inductances ensuring ZVS operations and a minimum voltage drop on the DC bus, are calculated. The voltage and current waveforms in the transformer are then calculated for the maximal values of leakage and magnetising inductances. Both analytical calculations and simulations are used. Several designs of transformers are then generated from these waveforms and for various values are calculated, including: current densities, magnetic flux density, number of turns in the windings and form factors.

The electrical parameters of MFT designs (parasitic capacitances, leakage and magnetising inductances) are calculated thanks to appropriate models [14].

To calculate the temperatures in the windings and in the core of the MFT on a mission profile, the journey and stop are considered separately. It is assumed that there is no stop phase during the journey. The journey comprises thus acceleration, cruising, coasting and braking phases (see Table. 1). The power is the same for coasting and stop phases, however, the temperature and, thus losses, are different.

For each MFT, the temperatures are estimated both during the journey assuming that the thermal steady state is reached, and during the stop phase. The journey temperature is calculated thanks to the calculated losses during acceleration, cruising, coasting and braking phases, weighted by their respective durations (Table 1). Excluding the stop phase from the journey increases the mean power absorbed by the converter during this phase. The temperature estimations are thus, a priori, pessimistic compared to reality.

Designs not complying with constraints (inductances, dimensions, weight and temperatures in the windings and in the core of the MFTs) are eliminated.

The next step is the calculation of the losses in the MFTs and in the MOSFETs. To do so, the currents in the transformers and semiconductors are calculated again with the refined parameters of the MFT designs complying with the constraints and for the four values of power of the mission profile.

The switching energies of the SiC MOSFETs are approximated by a second order polynomial from supplier data [15]. As ZVS operation is assumed, turn-on losses are neglected. The evolution of the on-state resistance of the MOSFET $R_{ds,on}$ in function of the junction temperature is calculated thanks to equation (1) [16]. Several iterations of loss calculations in the MOSFETs are required to reach the thermal steady state, assuming a fixed base plate temperature.

$$R_{ds,on}(T_j) = R_{ds,on}(T_{ref}) \left(\frac{T_j}{T_{ref}} \right)^{2.4} \quad (1)$$

The winding losses are estimated thanks to the models developed in [17] to take into account skin and proximity effects in Litz wires in core type MFTs. The magnetic losses are calculated for non-sinusoidal flux density, thanks to the improved generalised Steinmetz equation (IGSE) [18]. The dielectric losses are evaluated considering each voltage harmonic and using the parasitic capacitances and the dissipation factor of the insulating material. Details on the thermal calculations are available in [8].

The total losses in the R-SAB can then be calculated for the four values of power absorbed by the PETT on the mission profile. The weighted losses on the mission profile are eventually obtained. The transformer design ensuring the minimum losses of the DC/DC converter on the mission profile can be selected.

The full process is reiterated in all the considered frequency range to determine the optimal frequency and MFT design.

4 Application

A 2 MW PETT, designed for 15 kV/16.7 Hz infrastructure and a 1.8 kV traction bus, is considered. The intermediate bus voltage is fixed at 3.6 kV, thanks to the use of 3.3 kV SiC MOSFETs, proposed by Wolfspeed [15], in a three level NPC configuration on the primary side of the

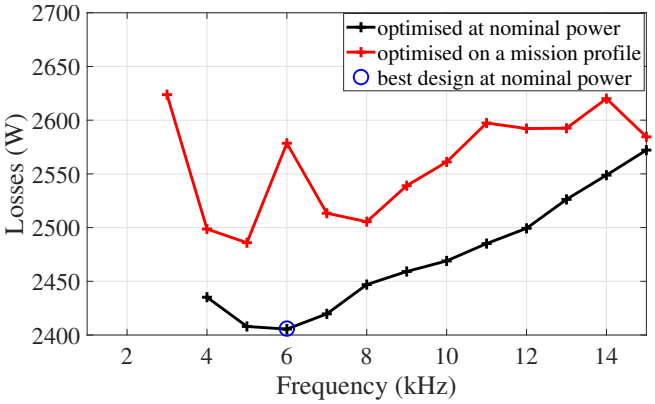

Fig. 5: Total losses at nominal power in the R-SAB for MFT designs leading to the lowest losses for each frequency.

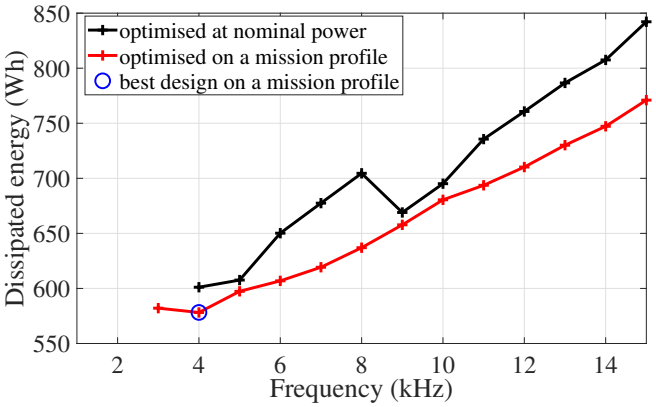

Fig. 6: Total dissipated energy on the mission profile in the R-SAB for MFT designs leading to the lowest losses for each frequency.

transformers. A minimum of eight active PEBBs, plus one added for redundancy, are necessary to withstand the 15 kV infrastructure voltage. In normal operation, eight PEBBs are active.

Cast resin insulation transformers with nanocrystalline C-core and laminated Litz wires are considered. They are cooled by forced air at 40 °C and 2 m/s. The base plates of the MOSFETs are assumed at 75 °C.

The constraints are the same as those considered in [9]. The maximal weight for the nine MFTs is set to 450 kg. The dimension constraints are imposed by the traction case geometry. One side of the MFT is limited by the length of the case divided by the number of MFTs. Fans and an air channel sufficient to dissipate the MFT losses limit the maximal height of the transformer.

The design of the R-SAB has been first optimised at nominal power. The optimisation has then been reiterated on the mission profile. The losses at nominal power and the total dissipated energy on the mission profile are shown Fig. 5 and Fig. 6. Then, the repartition of the losses in both designs at nominal power, and with only the power of the auxiliaries, i.e. during the stop phase, and the dissipated energy on the mission profile, are illustrated Fig. 7.

One can notice that the curves in Fig. 5 and Fig. 6 present significant variations, e.g. between 5 kHz and 6 kHz at nominal power for a MFT optimised on a mission profile, or between 8 kHz and 9 kHz on a mission profile for a design

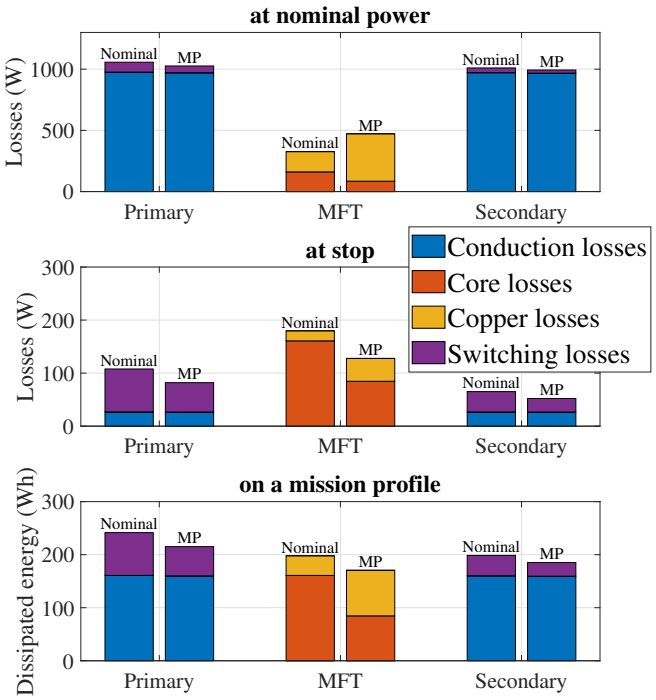

Fig. 7: Repartition of the losses at nominal power, at stop and of energy losses on the mission profile in the R-SAB designs optimised at nominal power and on the mission profile (MP).

optimised at rated power. This happens when one or several parameters (number of turns in the windings, current densities...) change between two consecutive frequencies to ensure a higher efficiency or to comply with the constraints.

The best MFT design, for an optimisation at nominal power, is obtained at 6 kHz. When optimised on the mission profile presented in Table 1, the lowest losses are reached at 4 kHz. At nominal power,

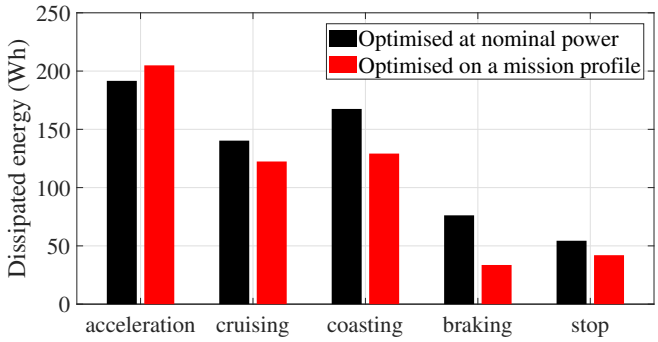

Fig. 8: Repartition of the dissipated energy on a typical journey, for a DC/DC optimised at nominal power and on a mission profile.

the losses in the DC/DC converter are 4 % higher in the converter optimised on the mission profile. However, the total dissipated energy on the mission profile is reduced by 13 % when optimised on a mission profile, compared to an optimisation at nominal power.

At nominal power (see Fig. 7), the main losses are copper losses in the MFT and conduction losses in the MOSFETs in both the primary and the secondary of the SAB. However, at low power (see Fig. 7), the MFT core losses and the switching losses in the MOSFETs are dominating, as they do not depend on the power. As power much lower than the nominal power is absorbed 64 % of the journey, i.e. during cruising and stop phases, the core losses in the transformer and the switching losses in the semiconductors are minimised when optimised on a mission profile, compared to an optimisation at rated power (see Fig. 7). As both switching losses and core losses increase with the frequency, design with lower weighted losses on the mission profile are obtained at lower frequency.

The repartitions of the losses during a 1 h typical journey for the designs optimised at nominal power and on a mission profile are shown Fig. 8. One can notice that during the acceleration phase, i.e. at nominal power, the losses are higher in the design optimised on a mission profile. However, the total losses on the mission profile are 13 % lower compared to the losses in the design optimised at rated power, thanks to a more suited optimisation in both the cruising, coasting and stop phases, leading to a gain on the losses of respectively 15 % and 30 %.

To minimise the dissipated energy on the mission profile, the core losses are minimised. The operating frequency and the core section are thus reduced. As the maximum flux density is limited by the core material, the number of turns increases to compensate the reduction of frequency and section. The copper losses are thus higher when optimised on a mission profile.

The volume and weight of both MFTs are the same, 49 kg/30 L, when optimised at rated power, and when optimised on the mission profile. These values correspond to the maximum constraints given to the optimisation algorithm. However, the core is smaller in the design optimised on a mission profile, while the windings are smaller in the design optimised at rated power. Thus, despite higher losses at rated power in the MFT optimised on a mission profile (see Fig. 7), lower temperatures can be reached with the same cooling system compared to the design optimised at rated power. Even if the losses in the windings are twice higher in the design optimised on a mission profile (see Fig. 7), the temperatures in the windings are lower thanks to lower current densities. However, the core losses, 60 % higher in the MFT optimised at rated power, lead to a higher core temperature compared to the design optimised on the mission profile.

5 Conclusions

In this paper, the design of an isolated DC/DC converter has been optimised both at rated power and on a typical mission profile for a regional train application. A 2 MW PETT using 3.3 kV SiC MOSFETs for a 15 kV/16.7 Hz infrastructure has been considered. A gain of 13 % on the total dissipated energy on the mission profile has been obtained by optimising the converter design on the mission profile instead of only at rated power. Moreover, the highest efficiency has been reached for a lower operating frequency, i.e. 4 kHz, when optimised on a mission profile compared to 6 kHz at rated power.

To improve this analysis, experimentations should be carried out on a prototype to validate the loss calculations, and especially the hypothesis on the MOSFET behaviour in soft switching.

The study is based on a loss comparison only. However, as the highest efficiency on a mission profile is obtained for a lower transformer frequency than for a design sized at rated power, some considerations on the acoustic noise should be included in further studies. However, this point is quite hard to estimate beforehand without a prototype.

The balancing of the intermediate capacitor bus mid-point should also require a few additional considerations.

The proposed approach can be applied for any solid state transformer application where the load varies in time, for example: railway power supply substations, distribution grid substations or photovoltaic.

Acknowledgment

This work has been supported by a grant overseen by the French National Research Agency (ANR) as part of the “Investissements d’Avenir" Program (ANE-ITE-002-01). The authors also gratefully acknowledge the support provided by Alstom.

6 References

[1] D. Dujic, F. Kieferndorf, and F. Canales, “Power electronic traction transformer technology for traction application - An overview”, in *Electronics*, vol. 16, 2012. DOI: 10.7251/ELS1216050D0.

[2] S. Farnesi, M. Marchesoni, and L. Vaccaro, “Advances in locomotive power electronic systems directly fed through AC lines”, in *International Symposium on Power Electronics, Electrical Drives, Automation and Motion (SPEEDAM)*, 2016. DOI: 10.1109/SPEEDAM.2016.7525932.

[3] J. Feng, W. Q. Chu, Z. Zhang, and Z. Q. Zhu, “Power electronic transformer based railway traction systems: challenges and opportunities”, *IEEE Journal of Emerging and Selected Topics in Power Electronics*, 2017. DOI: 10.1109/JESTPE.2017.2685464.

[4] B. Bednar, P. Drabek, and M. Pittermann, “The comparison of different variants of new traction drives with medium frequency transformer”, in *International Symposium on Power Electronics, Electrical Drives, Automation and Motion (SPEEDAM)*, 2016. DOI: 10.1109/SPEEDAM.2016.7525933.

[5] D. Ronanki and S. S. Williamson, “Evolution of power converter topologies and technical considerations of power electronic transformer-based rolling stock architectures”, *IEEE Transactions on Transportation Electrification*, 2018. DOI: 10.1109/TTE.2017.2765518.

[6] M. Steiner and H. Reinold, “Medium frequency topology in railway applications”, in *European Conference on Power Electronics and Applications*, 2007. DOI: 10.1109/EPE.2007.4417570.

[7] C. Stackler, F. Morel, P. Ladoux, A. Fouineau, F. Wallart, and N. Evans, “Optimal sizing of a power electronic traction transformer for railway applications”, in *44th Annual Conference of the IEEE Industrial Electronics Society (IECON)*, 2018. DOI: 10.1109/IECON.2018.8591686.

[8] F. Morel, C. Stackler, P. Ladoux, A. Fouineau, F. Wallart, *et al.*, “Power electronic traction transformers in 25 kV/50 Hz systems: Optimisation of DC/DC isolated converters with 3.3 kV SiC MOSFETs”, in *International Exhibition and Conference for Power Electronics, Intelligent Motion, Renewable Energy and Energy Management (PCIM Europe)*, 2019.

[9] C. Stackler, F. Morel, P. Ladoux, A. Fouineau, F. Wallart, *et al.*, “NPC assessment in insulated DC/DC converter topologies using SiC MOSFETs for power electronic traction transformer”, in *International Symposium on Power Electronics (Ee)*, 2019. DOI: 10.1109/PEE.2019.8923456.

[10] M. Marsilla, *FINE1 & OPEUS Final conference*, 2019.

[11] C. Zhao, D. Dujic, A. Mester, J. K. Steinke, M. Weiss, *et al.*, “Power electronic traction transformer-medium voltage prototype”, *IEEE Transactions on Industrial Electronics*, 2014. DOI: 10.1109/TIE.2013.2278960.

[12] R. Aceiton, J. Weber, and S. Bernet, “Input

filter for a power electronics transformer in a railway traction application", *IEEE Transactions on Industrial Electronics*, 2018. DOI: 10.1109/TIE.2018.2821621.

[13] P. Dworakowski, A. Wilk, M. Michna, B. Lefebvre, F. Sixdenier, and M. Mermet-Guyennet, "Effective permeability of multi air gap ferrite core 3-phase medium frequency transformer in isolated DC-DC converters", *Energies*, 2020. DOI: 10.3390/en13061352.

[14] A. Fouineau, "Méthodologies de conception de transformateurs moyenne fréquence pour application aux réseaux haute tension et réseaux ferroviaires", PhD thesis, Université de Lyon, France, 2019.

[15] J. Hayes, W. A. Curbow, B. Sparkman, D. Martin, K. Olejniczak, *et al.*, "Dynamic characterization of next generation medium voltage (3.3 kV, 10 kV) silicon carbide power modules", in *International Exhibition and Conference for Power Electronics, Intelligent Motion, Renewable Energy and Energy Management (PCIM Europe)*, 2017.

[16] K. Sheng, "Maximum junction temperatures of SiC power devices", *IEEE Transactions on Electron Devices*, 2009. DOI: 10.1109/TED.2008.2010605.

[17] A. Fouineau, M. Raulet, B. Lefebvre, N. Burais, and F. Sixdenier, "Semi-analytical methods for calculation of leakage inductance and frequency-dependent resistance of windings in transformers", *IEEE Transactions on Magnetics*, 2018. DOI: 10.1109/TMAG.2018.2858743.

[18] K. Venkatachalam, C. R. Sullivan, T. Abdallah, and H. Tacca, "Accurate prediction of ferrite core loss with nonsinusoidal waveforms using only Steinmetz parameters", in *IEEE Workshop on Computers in Power Electronics*, 2002. DOI: 10.1109/CIPE.2002.1196712.